



# A millimeter-wave end-fire dual-polarized array antenna with symmetrical radiation patterns and high isolation

Pengfei Yu<sup>1</sup> , Changning Wei<sup>2</sup> , Liguang Sun<sup>1</sup>, Zhuoqiao Ji<sup>2</sup>, Fan Yu<sup>1</sup>,  
Yi-Feng Cheng<sup>3</sup> and Lei Wang<sup>4</sup>

## Research Paper

**Cite this article:** Yu P, Wei C, Sun L, Ji Z, Yu F, Cheng YF, Wang L (2025) A millimeter-wave end-fire dual-polarized array antenna with symmetrical radiation patterns and high isolation. *International Journal of Microwave and Wireless Technologies* **17**(3), 389–397. <https://doi.org/10.1017/S1759078725000510>

Received: 8 March 2024

Revised: 4 April 2025

Accepted: 10 April 2025

### Keywords:

dual-polarized (DP); end-fire; LTCC; millimeter-wave (mmWave); mode-composite full-corporate-feed network

**Corresponding author:** Changning Wei;

Email: [weicn2023@szpu.edu.cn](mailto:weicn2023@szpu.edu.cn)

<sup>1</sup>Department of Electronic Engineering and Information Science, University of Science and Technology of China, Hefei, China; <sup>2</sup>Tech X Academy, Shenzhen Polytechnic University, Shenzhen, China; <sup>3</sup>School of Electronics and Information Engineering, Hangzhou Dianzi University, Hangzhou, China and <sup>4</sup>School of Engineering, Lancaster University, Lancaster, UK

## Abstract

This paper presents a millimeter-wave end-fire dual-polarized (DP) array antenna with symmetrical radiation patterns and high isolation. The DP radiation element is formed by integrating a quasi-Yagi antenna (providing horizontal polarization) into a pyramidal horn antenna (providing vertical polarization), resulting in a DP radiation element with a symmetrical radiation aperture. To efficiently feed the DP element while maintaining high isolation, a mode-composite full-corporate-feed network is employed, comprising substrate-integrated waveguide supporting the TE<sub>10</sub> mode and substrate-integrated coaxial line supporting the TEM mode. This design eliminates the need for additional transition structures, achieving excellent mode isolation and a reduced substrate layer number. A 1 × 4-element DP array prototype operating at 26.5–29.5 GHz using low temperature co-fired ceramic technology was designed, fabricated, and measured. The test results indicate that the prototype achieves an average gain exceeding 10 dBi for both polarizations within the operating band. Thanks to the symmetrical DP radiation element and mode-composite full-corporate-feed network, symmetrical radiation patterns for both polarizations are observed in both the horizontal and vertical planes, along with a high cross-polarization discrimination of 22 dB and polarization port isolation of 35 dB.

## Introduction

Dual-polarized (DP) array antennas can increase channel capacity and improve system reliability. Thus, they are favored in various millimeter-wave (mmWave) wireless applications, such as 5G and satellite communications [1, 2]. DP antennas can be divided into two categories depending on the radiation patterns: broadside and end-fire radiation. Most efforts are focused on DP antennas with broadside radiation. Patches [3, 4], cross slots/dipoles [5, 6] and magneto-electric (ME)-dipoles [7] are the main radiation structures to achieve DP broadside radiation. In comparison, end-fire DP antennas radiate electromagnetic energy parallel to the array plane, which is preferred in some specific applications, such as mobile terminals [8].

The low profile and narrow aperture of the end-fire antenna pose great challenges to the design of DP array antennas [9]. Therefore, in the design of end-fire DP array antennas, the integration of DP radiation elements and feeding networks are important factors to be considered. Recently, some impressive works have been done in this aspect in the mmWave band. Quasi-Yagi antennas fed by microstrip lines are utilized in paper [10] to realize the DP radiation. In contrast, substrate integrated waveguide (SIW) offers several advantages in the mmWave band, such as low loss and easy integration [11–14]. A DP full-corporate-feed network based on single-layer SIW is proposed in paper [11], with the DP radiation elements arranged alternately in a straight line. As an improvement, stacked SIWs are used to enhance the integration of the feeding networks [12–14]. In papers [12] and [13], both the polarizations require the mode coupling of the stacked SIWs, which limits the flexibility in their applications. In paper [14], separate radiators consisting of open-ended SIW antenna and printed dipole antenna are employed. However, the proposed composite DP radiation element has relatively poor cross-polarization discrimination (XPD) and polarization port isolation. By constructing DP antennas through two different radiation types, several mmWave end-fire DP array antennas have been reported in papers [15–17]. Unfortunately, these designs suffer from beam asymmetry or low isolation, due to the stacked DP radiation apertures in paper [15] or shared DP radiation apertures in papers [16, 17]. Designing an mmWave end-fire DP array antenna that exhibits symmetrical radiation patterns and high isolation (including port isolation and XPD) remains a challenge.

Additionally, all the works mentioned earlier are based on printed circuit board (PCB) technology, which limits the flexibility in multi-layer circuit layout. Compared with multilayer PCB, low temperature co-fired ceramic (LTCC) technology has better packaging characteristics and machining precision [18]. LTCC-based antennas are one of the mainstream choices for microsystems and antenna-in-package technology, and have received widespread attention. There are a few research reports on LTCC-based mmWave end-fire DP antennas [19–21]. However, they show narrow bandwidth [19] and large size [20]. A compact DP end-fire antenna fed by substrate integrated coaxial line (SICL) is introduced in paper [21], which achieves a significant improvement in port isolation and XPD. However, the operating bandwidths of the two polarizations are different. Moreover, the beam symmetry and feeding network integration also need to be improved.

To address the aforementioned challenges, this paper proposes an LTCC-based mmWave end-fire DP array antenna with a full-corporate-feed network. An optimized quasi-Yagi antenna is centrally inserted into the SIW pyramidal horn antenna to construct a new DP element, with low mutual interference between the two separate radiators. This produces symmetrical radiation patterns in horizontal polarization (H-pol) and vertical polarization (V-pol) with high XPD. By combining the SIW and SICL, a mode-composite (supporting TEM and  $TE_{10}$  mode) full-corporate-feed network is constructed to directly feed the DP radiation element. The proposed feeding network has the merits of a compact structure and high mode isolation. The fabricated prototype verifies that the designed antenna has the advantages of high integration, symmetrical radiation patterns, high XPD, and polarization port isolation.

## Antenna analysis and design

### Antenna configuration

The configuration of the proposed end-fire DP array antenna is shown in Fig. 1, which is designed using LTCC technology. The operating frequency band is 26.5–29.5 GHz, covering the 5G-mmWave NR band n257. The radiating section consists of  $1 \times 4$  DP elements with an extended substrate slab in the front. Air holes are drilled on the dielectric slab, which can enhance the impedance matching between the antenna and free space. Each DP element is a composite structure of a pyramidal horn antenna and a quasi-Yagi antenna (as presented in Fig. 2(a)). The period ( $p$ ) of the DP elements is set to 8.62 mm in this design, equivalent to 0.85 times the free space wavelength at the highest operating frequency (29.5 GHz). The feeding network contains a 1-to-4 mode-composite power divider and a mode splitter structure. The quasi-Yagi antenna is excited by TEM mode (in SICL) for H-pol, while the horn antenna is excited by  $TE_{10}$  mode (in SIW) for V-pol. These two modes are integrated in the mode-composite transmission line (MCTL) and transmit through the same physical channel. Based on the analysis of the electric field distribution characteristics and the high mode isolation of the TEM and  $TE_{10}$  modes in MCTL in paper [22], it can be seen that MCTL can not only reduce the complexity and substrate layer number of the DP feeding network but also help achieve high polarization isolation.

Ferro A6M ( $\epsilon_r = 5.9$  and  $\tan \delta = 0.002$ ) is adopted for the LTCC technology. All simulations are carried out using ANSYS HFSS.

### DP element

Figure 2 shows the 3D view and side view of the designed DP element fed by the SIW and SICL MCTL. It occupies 26 layers in total. The thickness of each substrate layer and metal layer is 100 and 8  $\mu\text{m}$ , respectively. The SIW horn antenna is used for the V-pol. To enhance the bandwidth, the horn antenna is optimized to a pyramidal shape. Although this shape requires various types of grounding metallized vias, which are difficult to achieve with traditional PCB technology, they can be easily achieved with LTCC. Interconnection between any layers can be achieved conveniently through the metallized vias by LTCC, making it feasible to implement the structure of the pyramid horn antenna and the DP radiation element proposed in this paper. For the feeding structure, it is necessary to minimize the interference between the  $TE_{10}$  mode (in SIW) and the TEM mode (in SICL). Therefore, the ratio of the width to the height of the SIW needs to be as large as possible. In this design, the width and height of the SIW are selected as 3.2 and 0.8 mm (Layers 10–17 in Fig. 2(b)). In addition, a substrate slab with air holes is loaded at the radiation aperture to reduce the effective relative dielectric constant [23]. The loading structure works as an impedance transformer to improve the impedance matching between the horn antenna and free space, since the characteristic impedance of air is much higher than the radiation impedance of the SIW horn antenna. The 3D radiation patterns of the single DP radiation element for both horizontal and vertical polarizations at 28 GHz are shown in Fig. 2(c). The simulated single-element gain exceeds 5.3 dBi for H-pol and 6.2 dBi for vertical polarization, with corresponding efficiencies exceeding 80% and 90%, respectively. The detailed design process of the DP radiation element is illustrated as follows.

The reflection coefficient curves in Fig. 3 demonstrate the effect of the substrate slab. The optimal dimensions of the pyramidal horn antenna are given in Figs. 2(b) and 3. The impedance matching bandwidth ( $|S_{11}| < -10$  dB) is effectively enlarged by substrate slab, covering 26–31 GHz.

The H-pol radiation is generated by a quasi-Yagi antenna, which is inserted into the central plane of the horn antenna (see in Fig. 2) to ensure the symmetry of the radiation patterns and reduce the influence on the horn antenna. The design evolution of the quasi-Yagi antenna is illustrated in Fig. 4. The reflection coefficient curves corresponding to the three models (Type-I, Type-II, and Type-III) are shown in Fig. 5. It originates from a dipole with a differential coplanar stripline (CPS) feeding structure (Type-I) (shown in Fig. 4(a)). The reflector and director are added to the back and front side of the dipole to achieve the radiation performance of a quasi-Yagi antenna. The endpoints of the reflector, dipole, and director are represented by  $t_1-t_1'$ ,  $t_2-t_2'$ , and  $t_3-t_3'$ , respectively. For Type-I, there is a significant electric field intensity at each of these points, as shown in Fig. 4(a). Type-I is a separate model of the quasi-Yagi antenna. The quasi-Yagi antenna is buried inside the LTCC, but there are no metallized vias around it. As a single-polarized antenna, it has good impedance matching performance in the design frequency band of 26.5–29.5 GHz. In Type-II, the quasi-Yagi antenna is integrated with the pyramidal horn antenna, necessitating the cutting of corners of the reflector. Meanwhile, the reflector is electrically connected to the metallized vias that form the side-wall of the pyramidal horn antenna. The modified quasi-Yagi antenna (Type-II) is shown in Fig. 4(b). The presence of the sidewall in the pyramidal horn antenna alters the distribution of electric field in proximity to the quasi-Yagi antenna, thereby modifying the antenna's equivalent capacitance distribution, as

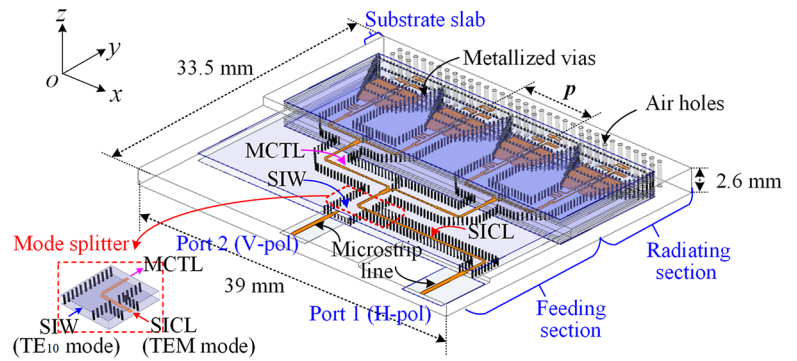


**Figure 1.** Configuration of the proposed end-fire DP array antenna.

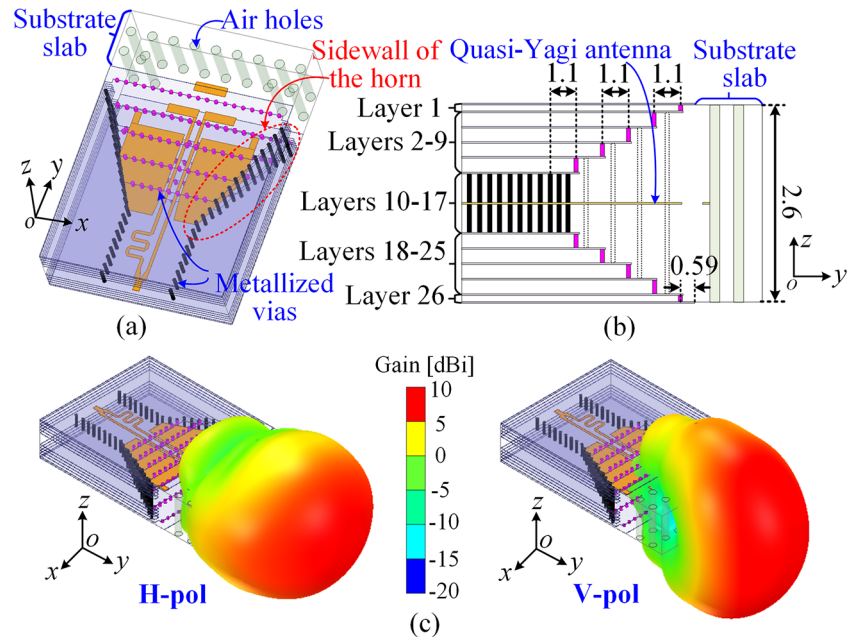


**Figure 2.** The single DP radiation element. (a) 3D view; (b) Side view (vias on the sidewall of the horn are illustrated by dashed lines); (c) 3D radiation patterns for H-pol and V-pol at 28 GHz. Dimension unit: mm.

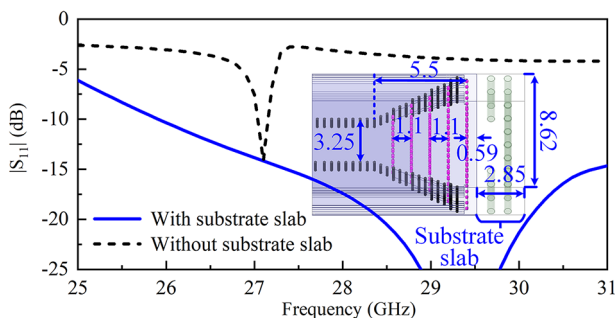


**Figure 3.** Simulated reflection coefficient of the SIW pyramidal horn (V-pol) with and without the substrate slab. Dimension unit: mm.

delineated in paper [24]. It can be seen from Fig. 4(b) that the electric field intensity is significantly reduced at the reflector endpoints  $t_1$  and  $t_1'$ . Therefore, Type-II suffers from a poor impedance matching. The comparison of the simulated reflection coefficients of Type-I and Type-II shown in Fig. 5 verifies this phenomenon. To mitigate this limitation, Type-III is proposed. The incorporation of two matching stubs along with chamfer processing on the reflector are utilized to fine-tune the equivalent capacitance distribution in the quasi-Yagi antenna. Figure 4(c) shows the refined structure of the quasi-Yagi antenna (Type-III). At the ends of the reflector

$t_1$  and  $t_1'$ , the symmetrically integrated matching stubs function as capacitive loading elements, facilitating charge accumulation, as explicated in paper [25]. Thus, the electric field intensity at  $t_1$  and  $t_1'$  in Type-III is increased and an electric field overlay similar to that of Type-I is obtained (shown in Fig. 4(c)). The corresponding simulated reflection coefficient is also plotted in Fig. 5. Compared with Type-II, the impedance matching of Type-III is significantly improved. The bandwidth of  $|S_{11}| < -10$  dB covers from 26.5 to 29.5 GHz.

A broadband microstrip-to-CPS balun is essential to excite the quasi-Yagi antenna. The proposed structure is illustrated in Fig. 6(a), formed by a microstrip T-junction power divider cascaded by two microstrip lines with different length to achieve the out-of-phase response. The simulated S-parameters of the balun are depicted in Fig. 6(b). In the frequency range of 26.5–29.5 GHz, acceptable amplitude and phase responses are obtained. The variations in amplitude distribution between the two output ports is less than 0.18 dB, and the corresponding phase difference ranges from  $170^\circ$  to  $188^\circ$ .

#### 1×4 DP antenna array

A  $1 \times 4$  mode-composite full-corporate-feed network is designed to support the proposed end-fire DP array antenna in Fig. 1. The structure of the feeding network is illustrated in Fig. 7(a). It consists

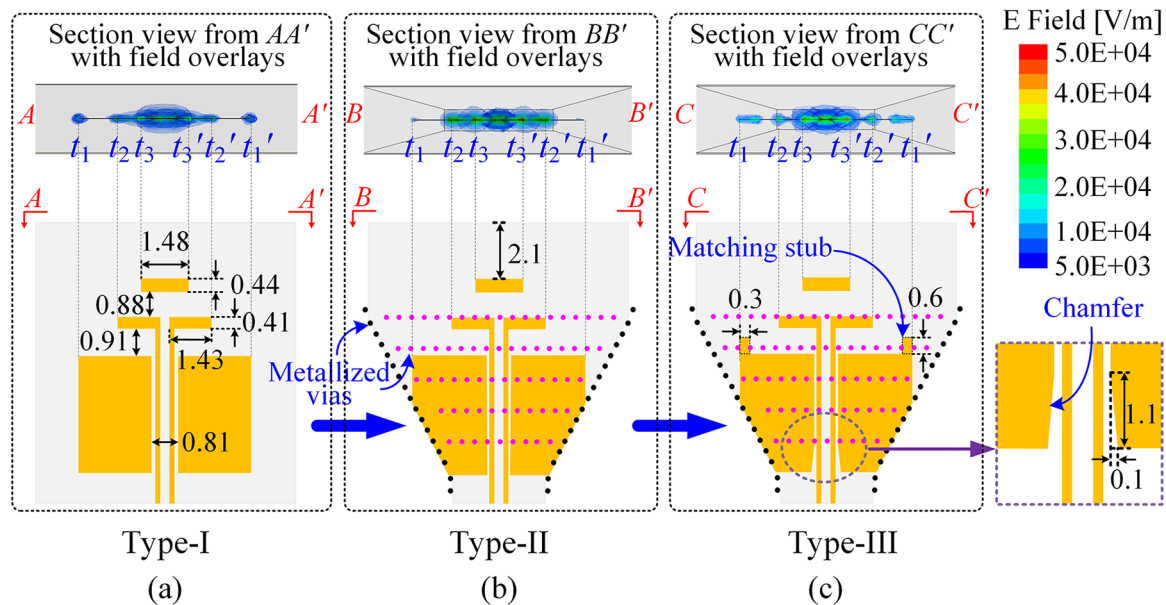


**Figure 4.** Design evolution of the quasi-Yagi antenna (H-pol) and the corresponding electric field overlays at 28 GHz in section view. (a) Initial model (Type-I); (b) Modified model integrated with the SIW pyramidal horn antenna (Type-II); (c) Final model after impedance matching optimization (Type-III). Dimension unit: mm.

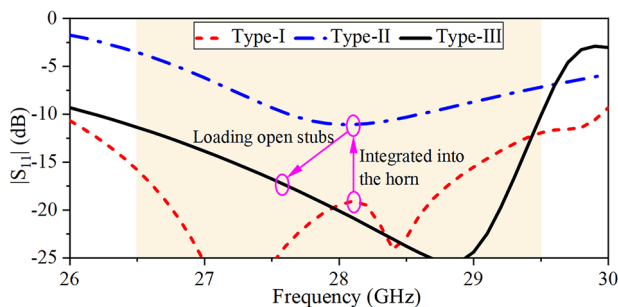


**Figure 5.** Simulated reflection coefficients of Type-I, Type-II, and Type-III.

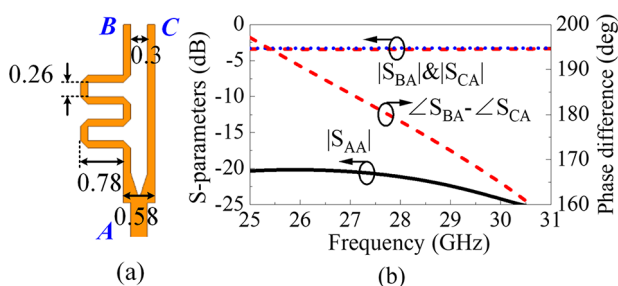


**Figure 6.** Microstrip-to-CPS balun. (a) Layout; (b) simulated S-parameters. Dimension unit: mm.

of a 1-to-4 MCTL-based power divider cascaded with a mode splitter. The 1-to-2 MCTL-based power divider (marked with a red frame), as the basic power divider unit, is used to implement the 1-to-4 power divider. The mode splitter (marked with a green frame) is realized by vertically inserted SIW and SICL. The gap on the sidewall of the SIW allows the strip of the SICL to pass through, and its width needs to be carefully optimized for better isolation and impedance matching. Figure 7(b) displays the simulated S-parameters of the mode-composite feeding network. In the

required frequency band of 26.5–29.5 GHz, a reflection coefficient of below  $-20$  dB and a transmission coefficient of  $-6.65 \pm 0.1$  dB are achieved for both the  $TE_{10}$  and TEM mode. In addition, the port isolation is up to 70 dB. Due to the equal-amplitude and in-phase feeding excitation used in the proposed  $1 \times 4$  element array antenna, the radiation direction is fixed along the  $y$ -axis in Fig. 1. In future research, if it is necessary to change the radiation direction of the antenna, phase adjustment structures, such as delay lines with different lengths, could be introduced [26].

## Experimental results

### Simulated and measured results

As shown in Fig. 8, a prototype is fabricated. The main dimensions of the antenna are 39 mm  $\times$  33.5 mm  $\times$  2.6 mm, with an additional space for the test fixture. The step on the antenna surface is a boundary formed by opening a cavity to reveal the internal feeding network region. The tapes from layer 1 to layer 9 and layer 18 to layer 26 in the feeding network area are all blank areas without circuit structures, which can be used to place active devices in the system integration or removed through cavity opening. As an example, the design in this paper removes the tapes from layer 1 to layer 9 in the feeding network area, exposing the surface of the layer 10 tape. At the same time, the 9 layers of tapes from layer 18 to layer 26 in the feeding network area are retained. Two 2.4-mm coaxial connectors are soldered to measure the reflection coefficients and radiation patterns of both polarizations, respectively.

The reflection coefficients and port isolation, both simulated and measured, are illustrated in Fig. 9. An Agilent N5244 network analyzer is used to obtain the measured results, which are reasonably consistent with the simulated results. The discrepancy can be primarily attributed to fabrication errors and the test fixture. In the frequency range of 26.5–29.5 GHz, it can be seen in Fig. 9 that the  $|S_{11}|$  and  $|S_{22}|$  are below  $-10$  dB for both polarizations. In addition, the  $|S_{21}|$  is lower than  $-40$  dB in simulation and  $-35$  dB in measurement.



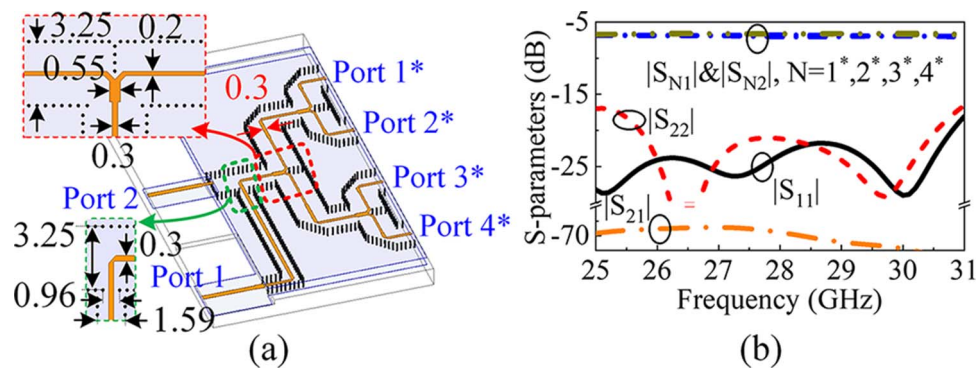


Figure 7. Mode-composite feeding network. (a) 3-D view; (b) responses. Dimension unit: mm.

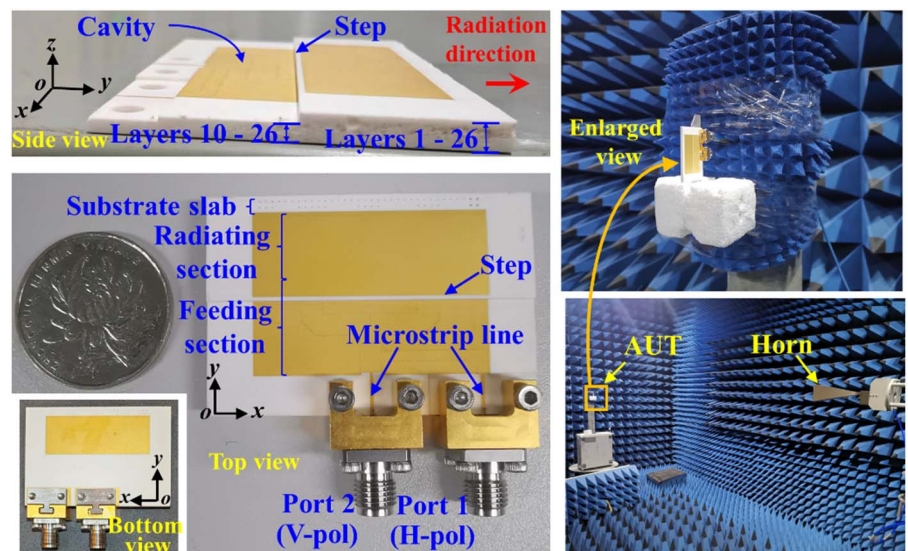


Figure 8. Photograph of the fabricated prototype and test environment.

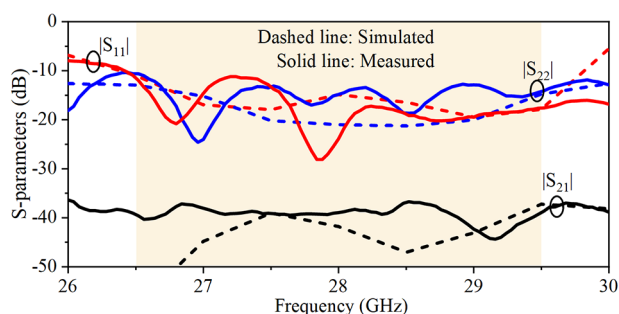


Figure 9. Simulated and measured S-parameters.

A far-field antenna measurement system is employed to test the radiation performance in an anechoic chamber, as shown in Fig. 8. The simulated and measured normalized radiation patterns at 26.5, 28, and 29.5 GHz for both polarizations are illustrated in Fig. 10. With the change of frequency, the main beam direction remains stable and symmetrical. The simulated and test results show that the 3 dB beam widths at the frequency points of 26.5, 28, and 29.5 GHz under Port 1 excitation (H-pol) are 14°, 14.6°, and 15.6° in the  $xoy$ -plane, respectively. The corresponding results in the  $yozy$ -plane are 96°, 92.2°, and 94°. When excited by Port 2 (V-pol), the 3 dB beam widths at the frequency points of 26.5, 28, and 29.5 GHz

in the  $xoy$ -plane are 16.1°, 16.3°, and 13.8°. And in the  $yozy$ -plane, the 3 dB beam widths are 100°, 92°, and 94.4°, respectively. For both polarizations, the simulated radiation pattern towards backward direction does not agree well with the measured one, due to the fixture of the antenna test system, which has a more significant effect on the relatively large backward radiation of the pyramidal horn antenna. In addition, the measured XPD is better than 22 dB across the operating frequency band.

The simulated and measured peak gains are illustrated in Fig. 11. For H-pol, the peak gain ranges from 9 to 11 dBi in simulation and varies from 8.6 to 10.8 dBi in measurement. For V-pol, the simulated and measured peak gains are 9.2–11.5 and 9–11.1 dBi. The measured peak gain is about 0.4 dB lower than the simulated value, mainly due to errors in the fabrication and measurement processes. As shown in Fig. 11, the total antenna efficiency is 66% to 80% for V-pol and 56% to 73% for H-pol over the entire required frequency band. This efficiency is approximated by dividing the measured peak gain by the simulated directivity.

### Comparison and discussion

Table 1 presents a comparison between the proposed antenna and other mmWave end-fire DP array antennas. All these designs are 1 × 4-element array antennas. The feeding networks in paper [10] are based on microstrips. As a single-layer structure, the

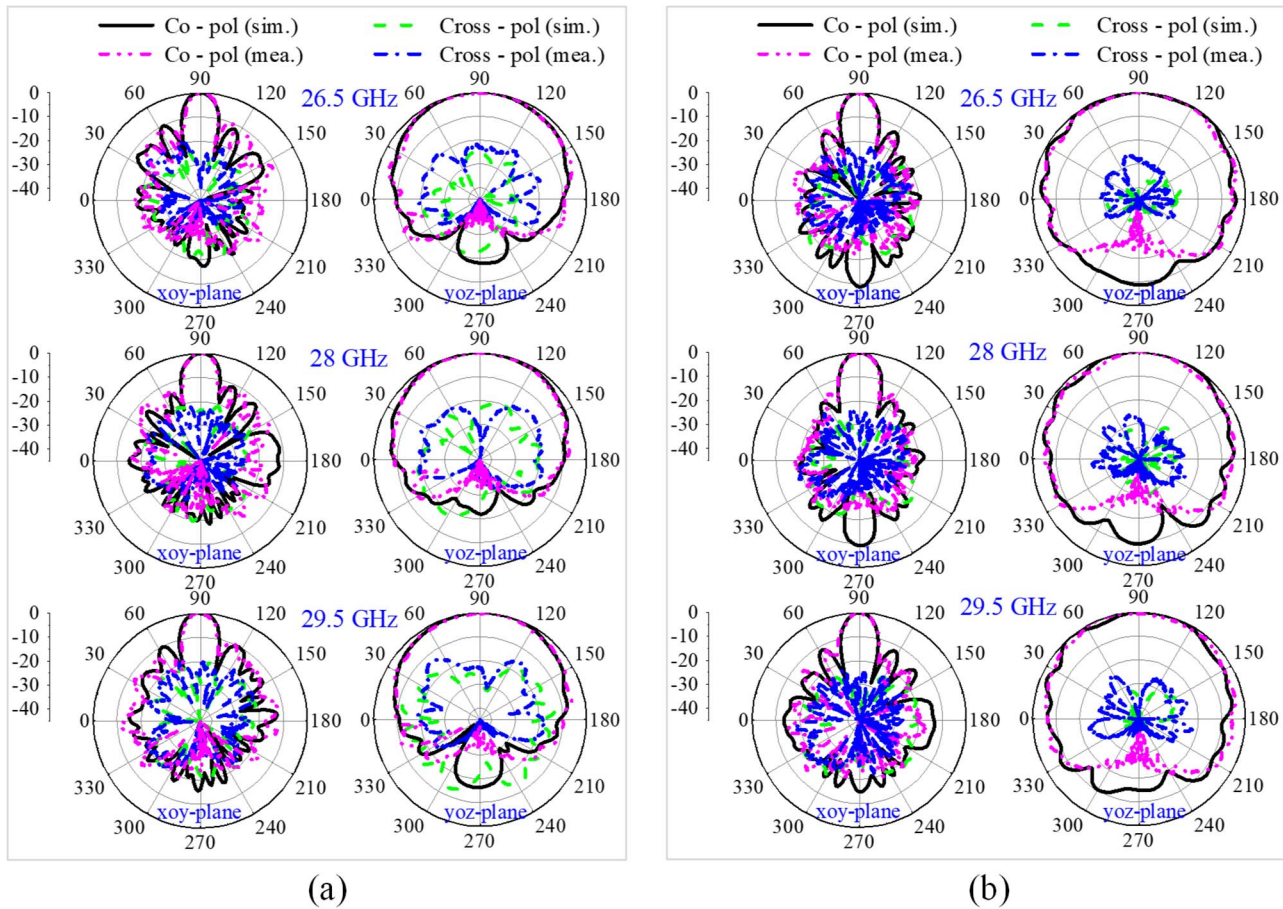


**Figure 10.** Simulated and measured normalized patterns. (a) With Port 1 excitation (H-pol); (b) with Port 2 excitation (V-pol).

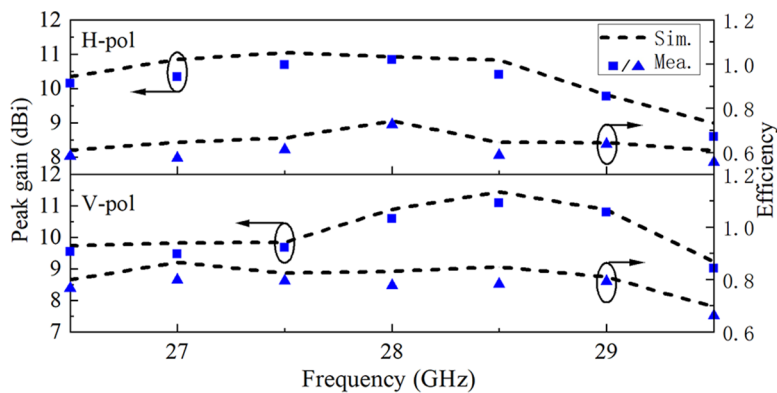


**Figure 11.** Simulated and measured peak gain, and calculated efficiency.

microstrips must be routed carefully to avoid interference between the two polarizations. Due to parasitic radiation in the mmWave band, the microstrip-based DP feeding network suffers from low port isolation. Stacked structures are adopted in works [14] (two stacked SIWs) [15], (stacked microstrip and SIW) and [21] (two stacked SICLs). These structures exhibit better DP integration and improved port isolation but are unfavorable for the structural symmetry of the antenna. Additionally, the implementation necessitates an increased number of layers. In this study, an enhancement has been made by integrating the H-pol feeding network

(SICL) with the V-pol feeding network (SIW) to establish a mode-composite DP feeding network. The integration results in a design characterized by exemplary DP integration, improved port isolation, symmetrical structure, and a reduction in the number of substrate layers.

Due to the asymmetrical DP radiation element, the antennas in papers [10, 15] and [21] have asymmetrical radiation patterns. In paper [14], two symmetrical dipoles are integrated into the upper and lower ground planes of the SIW antenna for symmetrical patterns, which results in high cross polarization simultaneously. In

**Table 1.** Comparison with other mmWave end-fire DP works

Ref.	Fabrication/Size <sup>a</sup> ( $\lambda_0^{-1}$ )	FN <sup>2</sup> /DP integration	Radiator/DP integration	$f_0^3$ (GHz)/BW <sup>4</sup> (%)	Gain <sup>b</sup> (dBi)	Isolation <sup>c</sup> /XPD (dB)	Symmetrical pattern
[10]	PCB/ $3.65 \times 1.54 \times 0.23$	MS <sup>5</sup> /Coplanar	Quasi-Yagi/Orthogonal	36/11.1	11	20/15	No
[14]	PCB/ $2.38 \times 1.2 \times 0.43$	SIW/Stacked	Dipole and SIW/Shared aperture	26/11.3	9	22/17	Yes
[15]	PCB/ $3.12 \times 1.77 \times 0.19$	MS and SIW/Stacked	Dipole and horn/Stacked	28/10.7	8	18/15	No
[21]	LTCC/ $2.24 \times 0.35 \times 0.12$	SICL/Stacked	Dipole and monopole/Orthogonal	28/6.1	8	30/19	No
This work	LTCC/ $3.4 \times 1.12 \times 0.24$	MCTL/Structure-shared	Quasi-Yagi and horn/Shared aperture	28/10.7	10	35/22	Yes

<sup>a</sup>Size of radiating section.<sup>b</sup>Average gain.<sup>c</sup>Port isolation. $\lambda_0^{-1}$ : free space wavelength at the center frequency, FN<sup>2</sup>: feeding network,  $f_0^3$ : center frequency, BW<sup>4</sup>: bandwidth, MS<sup>5</sup>: microstrip.

this study, the dipole is centrally inserted into the SIW pyramidal horn antenna. Through the aforementioned optimization, the mutual interference between the dipole and the SIW horn antenna is minimized, thereby achieving both symmetrical radiation patterns and high XPD.

In addition, the antennas in papers [10, 14] and [15] are based on PCB technology, while those in paper [21] and this study are based on LTCC technology. The LTCC-based antenna provides better performance in multi-layer layout and integration, especially in the mmWave band. The work in paper [21] fully utilizes the high integration advantages of the LTCC process, achieving the most compact size. Compared with that in paper [21], the proposed design not only realizes symmetrical radiation patterns characterized by high isolation (including both port isolation and XPD) but also exhibits an extended bandwidth and superior peak gain.

## Conclusion

This paper proposes an mmWave end-fire DP array antenna based on LTCC technology, featuring symmetrical radiation patterns and high isolation. The quasi-Yagi antenna (H-pol) and SIW pyramidal horn antenna (V-pol) are integrated into the same aperture to achieve a symmetrical DP radiation. The SIW and SICL are composited to form a mode-composite full-corporate-feed network, which offers the advantages of a reduced number of substrate layers and high mode isolation. For demonstration, a  $1 \times 4$ -element prototype is designed, fabricated, and measured. The features of DP operation with symmetrical radiation patterns, high isolation, and ease of integration make this antenna suitable for the applications in mmWave high-data-rate point-to-point wireless communication. The proposed antenna can be utilized in scenarios such as handheld mobile terminals, small satellites, and airborne antennas that require high system integration due to space constraints.

**Data availability statement.** The data that support the findings of this study are available on request from the corresponding author. The data are not publicly available due to privacy or ethical restrictions.

**Acknowledgements.** This work was supported by the Postdoctoral Later-stage Foundation Project of Shenzhen Polytechnic University under grant No. 6023271042K, the Scientific Research Startup Fund of Shenzhen Polytechnic University under grant No. 6024330002K and 6023312046K, and the Shenzhen Science and Technology Program under grant GJHZ20220913144203007 and GJHZ20240218113900001.

**Author contributions.** Pengfei Yu: Methodology; writing – original draft. Changning Wei: Writing – review and editing. Liguang Sun: Supervision and guidance. Zhuoqiao Ji: Software. Fan Yu: Test work. Yi-Feng Cheng: Validation. Lei Wang: Theoretical support.

**Competing interests.** The authors report no conflict of interest.

## References

- Jo J, Kim -J-J, Yoon J, Choi D and Hong W (2017) Exploitation of dual-polarization diversity for 5G millimeter-wave MIMO beam-forming systems. *IEEE Transactions on Antennas and Propagation* **65**, 6646–6655.
- Henarejos P and Pérez-Neira AI (2015) Dual polarized modulation and reception for next generation mobile satellite communications. *IEEE Transactions on Communications* **63**, 3803–3812.
- Wang M and Chan CH (2022) Dual-polarized, low-profile dipole-patch array for wide bandwidth applications. *IEEE Transactions on Antennas and Propagation* **70**, 8030–8039.
- Zakerifar H, Nourinia J and Ghobadi C (2024) Broadband dual-polarized antenna with parasitic elements for base-station applications. *International Journal of Microwave and Wireless Technologies* **16**, 1272–1282.
- Yang Q, Gao S, Luo Q, Wen L, Ban YL, Yang X, Ren X and Wu J (2020) Dual-polarized crossed slot array antenna designed on a single laminate for millimeter-wave applications. *IEEE Transactions on Antennas and Propagation* **68**, 4120–4125.
- Gao J, Li T, Wang H, Lei X and Wang K (2023) A compact dual-band dual-linearly polarized waveguide slot array antenna with groove at waveguide bottom. *International Journal of Microwave and Wireless Technologies* **15**, 1205–1211.
- Li Y, Wang C and Guo YX (2020) A Ka-band wideband dual-polarized magnetolectric dipole antenna array on LTCC. *IEEE Transactions on Antennas and Propagation* **68**, 4985–4990.
- Raghavan V, Chi M-L, Tassoudji MA, Koymen OH and Li J (2019) Antenna placement and performance tradeoffs with hand blockage in millimeter wave systems. *IEEE Transactions on Communications* **67**, 3082–3096.
- Cao Y, Cai Y, Wang L, Qian Z and Zhu L (2018) A review of substrate integrated waveguide end-fire antennas. *IEEE Access* **6**, 66243–66253.
- Hsu Y-W, Huang T-C, Lin H-S and Lin Y-C (2017) Dual-polarized quasi Yagi-Uda antennas with endfire radiation for millimeter-wave MIMO terminals. *IEEE Transactions on Antennas and Propagation* **65**, 6282–6289.
- Li A and Luk K-M (2020) Single-layer wideband end-fire dual-polarized antenna array for device-to-device communication in 5G wireless systems. *IEEE Transactions on Vehicular Technology* **69**, 5142–5150.



12. **Li A and Luk K-M** (2019) Millimeter-wave dual linearly polarized end-fire antenna fed by 180° hybrid coupler. *IEEE Antennas and Wireless Propagation Letters* **18**, 1390–1394.
13. **Zhu Y and Deng C** (2022) Millimeter-wave dual-polarized multibeam endfire antenna array with a small ground clearance. *IEEE Transactions on Antennas and Propagation* **70**, 756–761.
14. **Lu R, Yu C, Zhu Y and Hong W** (2020) Compact millimeter-wave endfire dual-polarized antenna array for low-cost multibeam applications. *IEEE Antennas and Wireless Propagation Letters* **19**, 2526–2530.
15. **Li H, Li Y, Chang L, Sun W, Qin X and Wang H** (2021) A wideband dual-polarized endfire antenna array with overlapped apertures and small clearance for 5G millimeter-wave applications. *IEEE Transactions on Antennas and Propagation* **69**, 815–824.
16. **Zhang J, Zhao K, Wang L, Zhang S and Pedersen GF** (2020) Dual-polarized phased array with end-fire radiation for 5G handset applications. *IEEE Transactions on Antennas and Propagation* **68**, 3277–3282.
17. **Khajeim MF, Moradi G, Shirazi RS and Zhang S** (2021) Broadband dual-polarized antenna array with endfire radiation for 5G mobile phone applications. *IEEE Antennas and Wireless Propagation Letters* **20**, 2427–2431.
18. **Wolff I, Günner C, Kassner J, Kulke R and Uhlig P** (2018) New heights for satellites: LTCC multilayer technology for future satellites. *IEEE Microwave Magazine* **19**, 36–47.
19. **Zhao Y and Zhao A** 2019 End-fire dual polarized 5G millimeter-wave antenna array for mobile devices. *IEEE Asia-Pacific Microwave Conference (APMC)*, Singapore.
20. **Yamashita D** 2021 LTCC end-fire array antenna with dual-band and dual-polarization for mobile International Symposium on Antennas and Propagation (ISAP), Taipei.
21. **Chou H-T, Chou S-J, Deng JDS, Chang C-H and Yan Z-D** (2022) LTCC-based antenna-in-package array for 5G user equipment with dual-polarized endfire radiations at millimeter-wave frequencies. *IEEE Transactions on Antennas and Propagation* **70**, 3076–3081.
22. **Sun K, Wang B, Yang T, Liu S, Chen Y, Zhao Y and Yang D** (2022) Dual-polarized millimeter-wave endfire array based on substrate integrated mode-composite transmission line. *IEEE Transactions on Antennas and Propagation* **70**, 341–352.
23. **Cai Y, Qian Z-P, Zhang Y-S, Jin J and Cao W-Q** (2014) Bandwidth enhancement of SIW horn antenna loaded with air-via perforated dielectric slab. *IEEE Antennas and Wireless Propagation Letters* **13**, 571–574.
24. **Abbosh A** (2013) Accurate effective permittivity calculation of printed center-fed dipoles and its application to quasi Yagi-Uda antennas. *IEEE Transactions on Antennas and Propagation* **61**, 2297–2300.
25. **Balanis CA** (2005) *Antenna Theory: Analysis and Design*. New Jersey: John Wiley & Sons.
26. **Mao C, Khalily M, Xiao P, Zhang L and Tafazolli R** (2021) High-gain phased array antenna with endfire radiation for 26 GHz wide-beam-scanning applications. *IEEE Transactions on Antennas and Propagation* **69**, 3015–3020.



**Pengfei Yu** received the B.S. and M.S. degree in electronic engineering in Zhejiang University, Hangzhou, China in 2010 and 2014, respectively. He is currently pursuing the Ph.D. degree in the University of Science and Technology of China, Hefei, China. His research interests include antenna techniques, RF circuits, and system integration.



**Changning Wei** received the B.S. degree in electronic engineering from the University of Science and Technology of China (USTC), Hefei, China, in 2014, and the Ph.D. degree from The Chinese University of Hong Kong, Hong Kong, in 2019. He is currently with the School of Tech X Academy, Shenzhen Polytechnic University, Shenzhen, China, as a Faculty Member. His research interests include RF integrated circuits, antenna decoupling techniques, massive multiple-

input multiple-output (MIMO) arrays, and signal processing for 5G/6G and satellite wireless communications.



**Ligu Sun** received the B.S. and Ph.D. degrees in electrical engineering from the University of Science and Technology of China in 1982 and 1991, respectively, and the M.S. degree in electrical engineering from the China Research Institute of Radio Wave Propagation in 1985. From 1995 to 1996, he was a Visiting Scholar with the Massachusetts Institute of Technology and Northeast University respectively in Boston of USA. From 1996 to 2000, he was a Senior Engineer and a Manager with DSC Ltd. (Tyco International Ltd) in Toronto of Canada. From 2000 to 2009, he was a Senior Staff Engineer with Sychip Inc. (Murata Manufacturing Company Ltd) in Dallas of USA. Since 2009, he has been a Full Professor with the University of Science and Technology of China in Hefei of China. His research interests include RF circuits/ devices/system integration, signal integrity, antenna, electromagnetic wave propagation and scattering, etc.

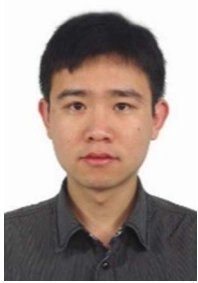


**Zhuoqiao Ji** received the B.S. degree in Information Engineering from the South China University of Technology in 2012. From 2012 to 2015, she was with Ericsson (China) Communications Co. Ltd. She received the Ph.D. degree in Electrical Engineering at City University of Hong Kong in 2022. She is currently with the Institute for Carbon-Neutral Technology from the School of Automotive and Transportation Engineering, Shenzhen Polytechnic University, Shenzhen, China, as a Faculty Member. Her current research interests include dielectric rod waveguide antennas, millimeter-wave and 5G/6G circularly polarized antennas for satellite wireless communications.





**Fan Yu** received the B.S. degree in electronic engineering in Xidian University, Xian, China, in 2022. He is currently pursuing the M.S. degree with the University of Science and Technology of China, Hefei, China. His current research interests include antenna decoupling techniques, and large-scale multiple-input multiple-output (MIMO) arrays.



**Yi-Feng Cheng** received the B.Eng. degree from the University of Electronic Science and Technology of China, Chengdu, China, in 2014, and the Ph.D. degree from The Chinese University of Hong Kong, Hong Kong, in 2020. He is currently an Associate Research Fellow in Hangzhou Dianzi University. His current research interests include microwave theory, antenna theory, RF circuit design, and GNSS anti-jamming techniques.



**Lei Wang** received the Ph.D. degree in electromagnetic field and microwave technology from the Southeast University, Nanjing, China in 2015. From 2014 to 2016, he was a Research Fellow in the Swiss Federal Institute of Technology (EPFL) in Lausanne, Switzerland. From 2016 to 2017, he was a Postdoc in the KTH Royal Institute of Technology in Stockholm, Sweden. From 2017 to 2020, he was an Alexander von Humboldt fellow in the Hamburg University of Technology in Hamburg, Germany. From 2020 to 2023, he was an Assistant Professor in the Heriot-Watt University in Edinburgh, United Kingdom. Since 2024, he is an Associate Professor (Senior Lecturer) in the Lancaster University in Lancaster, United Kingdom. His research includes antenna theory and applications, active electronically scanning arrays, integrated antennas and arrays, substrate-integrated waveguide antennas, leaky-wave antennas, wireless power transfer, and wireless propagations.